Figure 10. Plot of δ/ϕ and $(L/d)_{cr}$ against relative density of compaction.

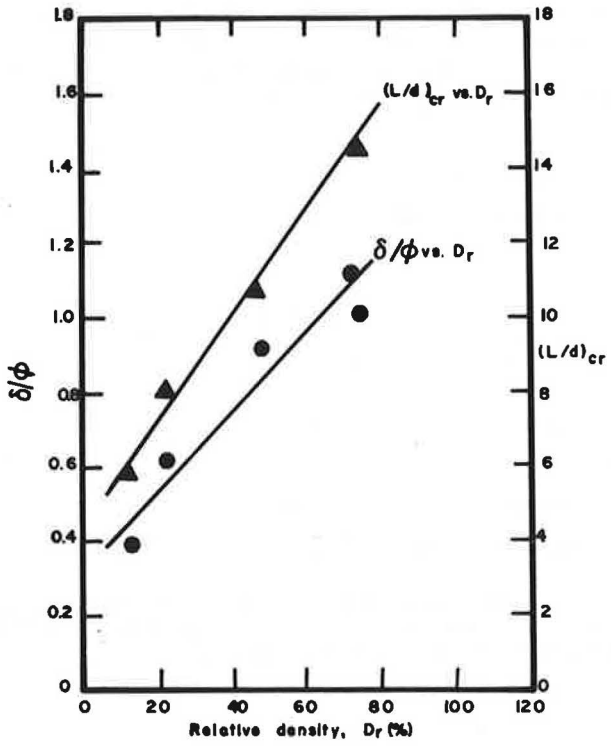

Figure 11. Procedure for determining critical embedment ratio.

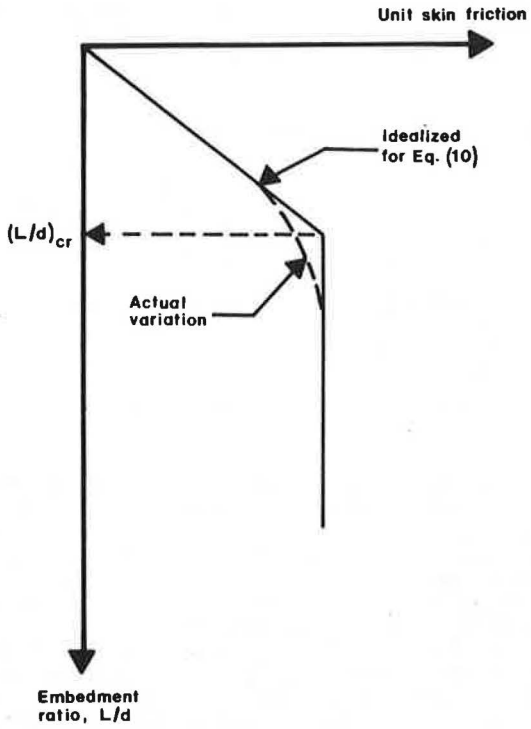

Mechanics and Foundation Engineering, Vol. 2, London, 1975, pp. 43-46.
5. R.F. Esquivel-Diaz. Pullout Resistance of Deeply Buried Anchors in Sand. M.S. thesis, Duke University, Durham, N.C., 1967.
6. V.A. Sowa. Pulling Capacity of Concrete Cast In Situ Bored Piles. Canadian Geotechnical Journal, Vol. 7, 1970, pp. 482-493.
7. B.M. Das and G.R. Seeley. Uplift Capacity of Pipe Piles in Saturated Clay. Soils and Foundations, The Japanese Society of Soil Mechanics and Foundation Engineering, Vol. 22, No. 1, 1982, pp. 91-94.

Publication of this paper sponsored by Committee on Foundations of Bridges and Other Structures.

Analysis of a Spiling Reinforcement System in Soft-Ground Tunneling

S. BANG

An investigation of a spiling reinforcement system used for stabilizing tunnels is presented. The system is composed of a series of radially installed reinforcing spiles placed around the perimeter of the tunnel heading before excavation. This system provides immediate stabilization of an opening as well as permanent stabilization. It has been successfully used for tunneling in weak rock formations and, to a lesser extent, in soft grounds. To date, no rational design methodology has been formulated because no reasonable analytic method of analysis has been suggested. A generalized plane strain composite finite-element analysis, which uses the proper simulation of the excavation and reinforcement to calculate three-dimensional stresses and displacements while the finite-element grid remains in two dimensions, is presented. The effects of the reinforcement, the inclination, and the spacing of the spiles on the performance of the system have been analyzed with the proposed method. The ground surface movements are used to calculate the vertical and horizontal distortions that are directly related to damage to buildings located above the tunnel.

A spiling reinforcement system has been successfully used in tunneling to strengthen weak rock formations as well as other soft grounds (1). The system typically consists of a series of radially installed 15- to 20-ft reinforcing spiles spaced from 2.5 to 5 ft with an inclination angle of approximately 30

degrees to the tunnel axis. The reinforcing spiles are formed by inserting rebars 1 to 1.5 in. in diameter in predrilled holes with subsequent grout. Figure 1 shows a schematic representation of the system. The general principle is to stabilize a

Figure 1. Spiling reinforcement ahead of the face.

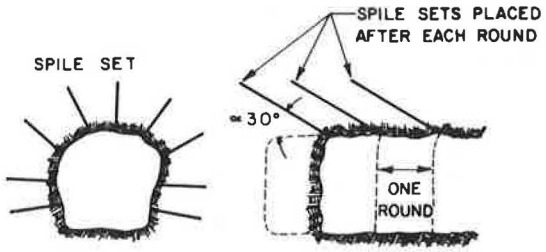

weak mass by installing an annular spiling reinforcement network along the perimeter of the tunnel heading before excavation. The reinforcing network is extended into the in situ ground both radially and longitudinally; therefore, the tunneling operation is always performed inside a tubular reinforced zone encircling the tunnel opening.

It has been reported (1) that the use of this scheme helps control both the immediate stabilization of an opening by preventing loosening and the permanent stabilization by restricting deformations. To date, a rational design methodology has not been formulated nor has a reasonable analysis procedure been offered. A method of analysis together with results obtained from the analysis for a spiling reinforcement system in soft-ground tunneling are presented here.

METHOD OF ANALYSIS

In formulating a method of analysis, it is important to take into consideration the tunnel excavation process and the soil-reinforcement composite behavior. These factors, which greatly influence the performance of the spiling reinforcement system, favor the use of finite-element analysis.

A generalized plane strain finite-element method has been developed to investigate the detailed behavior of the spiling reinforcement system. The generalized plan strain condition assumes three nonzero displacement components, none of which is dependent on the out-of-plane coordinate; thus the out-of-plane strain remains zero, and the displacement does not remain zero, which is commonly the case in the conventional plane strain approach. This approach was chosen because the conventional plane strain approach cannot effectively capture the out-of-plane behavior of the inclined spiling reinforcement, and a full three-dimensional analysis may be prohibitively expensive and time consuming. The main advantage of the generalized plane strain approach is that it calculates three-dimensional stresses and displacements while the finite-element grid remains in two dimensions. A brief description of the element stiffness matrix formulaton in a generalized plane strain condition follows.

The total virtual work is defined as

$$\delta V = \sum_{e=1}^{N} \delta V_e = \sum_{e=1}^{N} (\delta U_e - \delta W_e) = 0 \tag{1}$$

where N is the number of elements and δU_e and δW_e are the element virtual internal energy and external work, respectively. With an incremental material law,

$$\Delta \underset{\sim}{\sigma} = \underset{\sim}{C}\, \Delta \underset{\sim}{\epsilon} \tag{2}$$

where $\Delta\underset{\sim}{\sigma}$ and $\Delta\underset{\sim}{\epsilon}$ are vectors of small changes in stresses and strains and the constitutive matrix $\underset{\sim}{C}$ is dependent on current stress state and history, the element virtual internal work is written incrementally as

$$\delta \Delta U_e = \int_{V_e} \delta \underset{\sim}{\epsilon}^T \Delta \underset{\sim}{\sigma}\, dV_e \tag{3}$$

Using the incremental constitutive law, one can write

$$\delta \Delta U_e = \int_{V_e} \delta \underset{\sim}{\epsilon}^T \underset{\sim}{C}\, \Delta \underset{\sim}{\epsilon}\, dV_e \tag{4}$$

Because the displacement components in generalized plane strain are independent of the coordinate in the out-of-plane direction, z, i.e.,

$$\begin{aligned} u &= u(x,y) \\ v &= v(x,y) \\ w &= w(x,y) \end{aligned} \tag{5}$$

the strain components become

$$\underset{\sim}{\epsilon} = \left\{ \partial u/\partial x,\ \partial v/\partial y,\ 0,\ \partial u/\partial y + \partial v/\partial x,\ \partial w/\partial x,\ \partial w/\partial y \right\}^T \tag{6}$$

Using linear approximation of displacements, the three displacements at each node of the quadrilateral element can be approximated as

$$\begin{aligned} u &= \sum_{i=1}^{4} N_i u_i \\ v &= \sum_{i=1}^{4} N_i v_i \\ w &= \sum_{i=1}^{4} N_i w_i \end{aligned} \tag{7}$$

where u_i, v_i, and w_i are approximate nodal displacements and N_i is the first-order shape function.

From Equations 6 and 7 the strain component along x direction can be calculated as

$$\epsilon_x = \partial u/\partial x = (\partial/\partial x)\left(\sum_{i=1}^{4} N_i u_i \right) = \sum_{i=1}^{4} F_i u_i \tag{8}$$

where $F_i = \partial N_i/\partial x$.

Similarly, one can obtain

$$\begin{aligned} \epsilon_y &= \sum_{i=1}^{4} G_i v_i \\ \gamma xy &= \sum_{i=1}^{4} (G_i u_i + F_i v_i) \\ \gamma xz &= \sum_{i=1}^{4} F_i w_i \\ \gamma yz &= \sum_{i=1}^{4} G_i w_i \end{aligned} \tag{9}$$

where $G_i = \partial N_i/\partial y$.

The strain-displacement relationships can be written as

$$\Delta \underset{\sim}{\epsilon}_e = \underset{\sim}{B}\, \Delta \underset{\sim}{u}_e \tag{10}$$

where $\Delta\underset{\sim}{u}_e$ is vector of nodal displacement increments.

Equation 4 can then be rewritten as

$$\begin{aligned} \delta \Delta U_e &= \int_{V_e} [(\underset{\sim}{B}\delta \underset{\sim}{u}_e)^T \underset{\sim}{C} (\underset{\sim}{B} \Delta \underset{\sim}{u}_e)]\, dV_e \\ &= \delta \underset{\sim}{u}_e^T \underset{\sim}{K}\, \Delta \underset{\sim}{u}_e \end{aligned} \tag{11}$$

where the element tangent stiffness matrix $\underset{\sim}{K}$ is expressed as

$$\underset{\sim}{K} = \int_{V_e} \underset{\sim}{B}^T \underset{\sim}{C}\, \underset{\sim}{B}\, dV_e \tag{12}$$

Here

$$\underset{\sim}{B} = \begin{bmatrix} \underset{\sim}{F}^T & \underset{\sim}{0}^T & \underset{\sim}{0}^T \\ \underset{\sim}{0}^T & \underset{\sim}{G}^T & \underset{\sim}{0}^T \\ \underset{\sim}{0}^T & \underset{\sim}{0}^T & \underset{\sim}{0}^T \\ \underset{\sim}{G}^T & \underset{\sim}{F}^T & \underset{\sim}{0}^T \\ \underset{\sim}{0}^T & \underset{\sim}{0}^T & \underset{\sim}{F}^T \\ \underset{\sim}{0}^T & \underset{\sim}{0}^T & \underset{\sim}{G}^T \end{bmatrix} \tag{13}$$

where $\underset{\sim}{F}^T = \{F_1, F_2, F_3, F_4\}$ and $\underset{\sim}{G}^T = \{G_1, G_2, G_3, G_4\}$. Thus a 12 x 12 element tangent stiffness matrix can be obtained.

COMPOSITE ELEMENT

The composite representation of the reinforced system used in this analysis is an expansion of the approach developed by Romstad et al. (2), which expresses the orthotropic composite material properties as functions of the properties of each of the constituent materials (i.e., the soil mass, the reinforcing members, and their geometric arrangement).

This approach is based on the concept of the unit cell, an isolated small unit of the material that completely exhibits its composite characteristics. The average values of the stresses distributed over the cell faces are equal to the stresses in the equivalent composite material, and the average values of strains for the cell are those of the composite. Thus the average response of the unit cell to a homogeneous state of composite stress or strain is the same as the composite response of the material. Therefore, the desired composite properties may be calculated from detailed consideration of the behavior of the unit cell. These composite properties may then be used in the analysis of the complete structure. Such as analysis yields the composite stress and strain throughout the structure. Once the composite stress state is determined at a particular point in the structure, the corresponding constituent stress state (e.g., soil or spile) may be determined by returning to the analysis of the unit cell.

A schematic representation of the unit cell is shown in Figure 2. The composite material consists of a soil reinforced with spiles parallel to one another at a chosen spacing, S, and extending deep into the soil mass. The 1-axis in Figure 2 is chosen parallel to the spile and the 2- and 3-axes form a plane perpendicular to the longitudinal axis of the spile, where the 2-axis passes through the center of the tunnel. For a given reinforcing pattern, all spiles in a given 1-2 plane are assumed to be equally spaced.

The basic composite properties defining the stress-strain relationship were calculated by Romstad et al. (2) by successively considering a number of simple composite stress-strain states and approximately determining the response of the unit cell. The constitutive relationship in global coordinates can be obtained by considering two successive general two-dimensional axes rotations described by Mohr's circle relations (see Figure 3).

Figure 2. Unit cell.

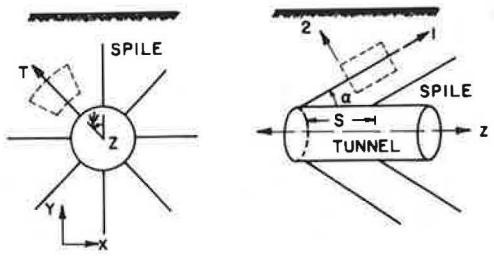

SHOTCRETE LINING

To prevent soil fall-out, a thin shotcrete lining may be used immediately after excavation and before installation of a permanent lining. The shotcrete lining was considered to be a flexible membrane element with no bending stiffness. Figure 4 shows a general membrane element with a thickness, t. This approach was chosen because the shotcrete lining is relatively thin and no separate representation of the lining in the finite-element grid is necessary in this approach. The resulting stiffness matrix of the membrane element can be added directly to that of the soil element adjacent to the lining.

Figure 3. Coordinate transformation of unit cell.

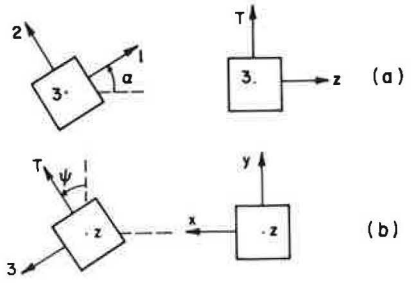

Figure 4. Membrane element representation.

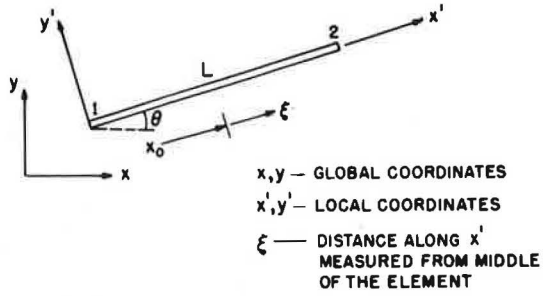

Assuming $\sigma_{y'}$, $\tau_{x'y'}$, and $\tau_{y'z'}$ are zero, the stress-strain relationship reduces to

$$\begin{bmatrix} \sigma_{x'} \\ \sigma_{z'} \\ \tau_{x'z'} \end{bmatrix} = \begin{bmatrix} C_{11} & C_{12} & 0 \\ C_{12} & C_{22} & 0 \\ 0 & 0 & C_{33} \end{bmatrix} \begin{bmatrix} \epsilon_{x'} \\ \epsilon_{z'} \\ \gamma_{x'z'} \end{bmatrix} \tag{14}$$

Taking the x' and z' displacements at any point as u' and w', respectively,

$$\epsilon_{x'} = \partial u'/\partial x'$$

$$\epsilon_{z'} = \partial w'/\partial z' = 0$$

$$\gamma_{x'z'} = (\partial u'/\partial z') + (\partial w'/\partial x') = \partial w'/\partial x' \tag{15}$$

are obtained. Note that the generalized plane strain condition is applied.

Because $x' = x_o + \xi(\ell/2)$ (from Figure 4),

$$\partial/\partial x' = (\partial/\partial\xi)(\partial\xi/\partial x') = (2/\ell)(\partial/\partial\xi) \quad (16)$$

Also

$$u' = [(1/2)\, u_1'(1 - \xi)] + [(1/2)\, u_2'(1 + \xi)]$$
$$= (1/2)\, [(u_2' + u_1') + \xi(u_2' - u_1')]$$

$$w' = (1/2)\, [(w_2' + w_1') + \xi(w_2' - w_1')] \quad (17)$$

The nodal displacements are expressed as

$$u_i' = u_i \cos\theta + v_i \sin\theta$$
$$v_i' = -u_i \sin\theta + v_i \cos\theta$$
$$w_i' = w_i \quad (18)$$

for i = 1, 2, where u, v, and w are the nodal displacements with respect to the x, y, and z coordinates. Substituting Equations 15 into the element virtual internal work expression, the following element stiffness matrix is obtained.

$$\underset{\sim}{K} = \begin{bmatrix} S_{11} & S_{12} & 0 & -S_{11} & -S_{12} & 0 \\ S_{12} & S_{22} & 0 & -S_{12} & -S_{22} & 0 \\ 0 & 0 & S_{33} & 0 & 0 & -S_{33} \\ -S_{11} & -S_{12} & 0 & S_{11} & S_{12} & 0 \\ -S_{12} & -S_{22} & 0 & S_{12} & S_{22} & 0 \\ 0 & 0 & -S_{33} & 0 & 0 & S_{33} \end{bmatrix} \quad (19)$$

where

$$S_{11} = (t/\ell)\, C_{11} \cos^2\theta$$
$$S_{12} = (t/\ell)\, C_{11} \cos\theta \sin\theta$$
$$S_{22} = (t/\ell)\, C_{11} \sin^2\theta$$

and

$$S_{33} = (t/\ell)\, C_{33}$$

INCREMENTAL ITERATIVE PROCEDURE

A finite-element computer program incorporating the previously mentioned features was developed. The construction and excavation process was simulated by a two-step incremental procedure. The first increment computes the initial stress state of the whole soil mass simulating in situ soil condition. This increment results in the development of stresses only (i.e., displacements are reset to zero). The second increment handles installing the spiles and excavating the tunnel as well as the construction of the shotcrete lining.

Within each increment, the nonlinear soil properties are accounted for by an iterative solution procedure using a nonlinear soil model developed by Duncan and Wong (3). This model assumes that the soil does not experience any stress- or strain-induced anisotropy (i.e., soil behavior is described by the instantaneous value of Young's modulus dependent on the stress state). A hyperbola is assumed to represent the stress-strain relationship for primary loading, and a straight line is assumed for unloading and reloading. A constant Poisson's ratio of 0.3 was used because the expressions for initial and tangent Poisson's ratio do not include the effect of unloading.

To improve the rate of convergence in the iteration process, a modified estimate of the soil modulus was used. For iteration n this value was expressed in terms of the calculated modulus and the modulus from the previous iteration, n - 1. That is,

$$E^{*(n)} = rE^{(n)} + (1 - r)E^{(n-1)} \quad (20)$$

where r is a relaxation factor. Because the convergence was oscillatory, a study was conducted to obtain the factor that gives the minimum number of iterations to be solved in the finite-element analysis. A factor of 0.7 was found. Using this underrelaxation factor, the solution usually converged within 4 to 8 iterations for each increment.

RESULTS

To understand the spiling reinforcement system in soft-ground tunneling, an investigation has been performed using the developed computer program. The investigation was limited to the study of a horizontal, single, circular tunnel with all spiles having the same axial and circumferential spacing and the same inclination angle along the entire circumference of the tunnel. Figure 5 shows the typical finite-element grid used in the study. The pertinent soil properties adopted in the study are given in Table 1.

Figure 5. Typical finite-element grid.

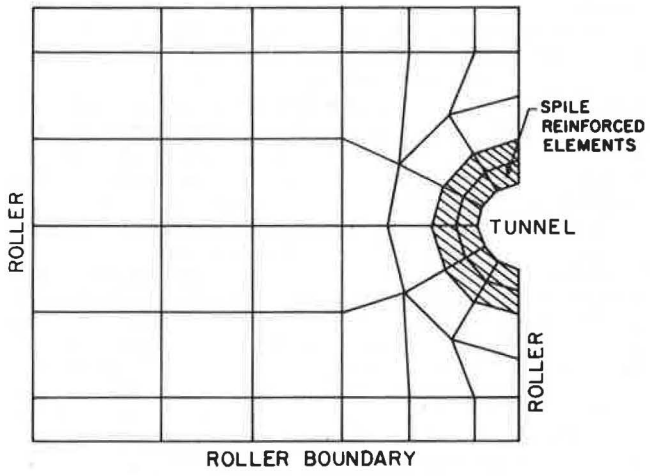

Table 1. Pertinent soil properties (4).

	Soils		
	No. 1 (SM[a])	No. 2 (CL[b])	No. 3 (CL[b])
Loading modulus	200	120	60
Unloading modulus	330	198	153
Modulus exponent	0.6	0.45	0.45
Failure ratio	0.7	0.7	0.7
Cohesion (psi)	2.778	2.083	0.694
Friction angle (°)	33	30	30
Poisson's ratio	0.3	0.3	0.3

[a]SM is silty sand.
[b]CL is clay with low plasticity.

The main variables considered were the depth of the tunnel center (H), the spacing (S), and the inclination of the spiles (α). Both the diameter of the tunnel and the length of the spiles remained constant at 20 ft. These values were chosen because the diameters of the tunnels used in Washington, D.C., Metro; Frankfurt; Sao Paulo; and San Francisco

were in the range of 18 to 21 ft (4) and, for the soil region farther than one radius from the opening, any increase in strength related to the presence of the reinforcement is small (5). (Note that spiles equal in length to the diameter of the tunnel with 30 degree inclination form a reinforced zone one radius from the tunnel opening.) The reinforcing spiles consisted of 1-in.-diameter rebars in 4-in. predrilled holes filled with grout. A brief description of the results obtained from the analysis follows.

Generally, there is a dramatic reduction in deformations when the spiling reinforcement system is used. Figure 6 shows a comparison of the tunnel deformations for unreinforced and reinforced tunnels. Quantitative comparisons of the deformation are given in Table 2. It is obvious that the use of spiling reinforcement reduces the crown and bottom movements of the tunnel by approximately 87 percent and 48 percent, respectively. A similar reduction in vertical ground surface movements is shown in Figure 7. The reduction may be as great as 90 percent of the unreinforced case.

To evaluate the stability of structures located above or adjacent to the tunnel, vertical and horizontal distortions were calculated and compared. The vertical distortion is defined as the differential vertical movement between two points divided by the distance separating them. The horizontal distortion is defined in a similar manner for the differential horizontal movement. These parameters have been used to describe the possible damage potential of various types of structures (6-10). Figure 8 shows the distribution of the vertical distortions for unreinforced and reinforced tunnels. Maximum vertical distortion of 1.25 percent results for the unreinforced tunnel, whereas only 0.12 percent is observed for the reinforced tunnel--a 90 percent reduction. According to Bjerrum (11), cracking in panel walls is to be expected if vertical distortion exceeds 0.33 percent. Similar reductions are observed in maximum horizontal distortions (i.e., 0.79 percent and 0.065 percent, respectively). According to O'Rourke et al. (12), 0.3 percent is the threshold value of horizontal distortion causing architectural damage in buildings.

The relative significance of the spile inclination angle to the performance of the system can be seen in Figure 9, which shows the resulting deformation of the tunnel due to different angles of spile inclination. Note that different scales are used for the tunnel and the displacement. An angle of spile inclination of approximately 30 degrees to the tunnel axis produces the least movement at the crown, the bottom, and the side of the tunnel. This finding can be further confirmed by comparing the ground surface distortions. The results indicate that an inclination angle of 30 degrees produces approximtely 30 percent less vertical distortion than an inclination angle of 40 degrees and approximately 5 percent less than an inclination angle of 20 degrees.

The effect of the spile spacing, a measure of the reinforcing intensity, has also been studied. A summary of the tunnel deformations obtained with different spile spacings is given in Table 3. The reduction in crown movement is much larger than the reduction in bottom movement, and the rate of improvement increases as spile spacing is reduced. The effect of spile spacing is even more pronounced in reducing the ground surface settlement. For in-

Figure 6. Deformation of the tunnel.

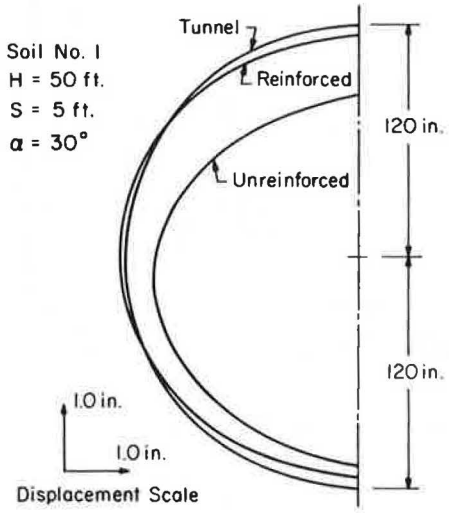

Figure 7. Vertical ground surface movement.

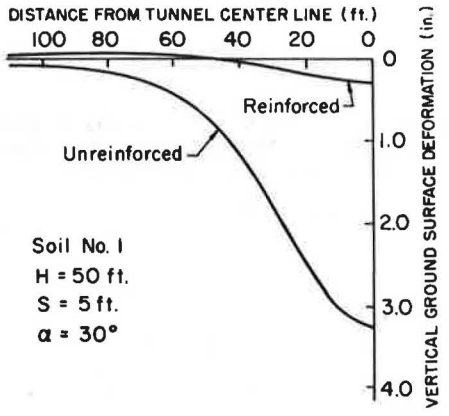

Table 2. Reduction of tunnel deformation spiling reinforcement in soil No. 1 (H = 50 ft).

	Unreinforced (in.)	Reinforced (in.)	Reduction (%)
Crown	-4.439	-0.5734	87
Bottom	1.4	0.7214	48

Figure 8. Vertical ground surface distortion.

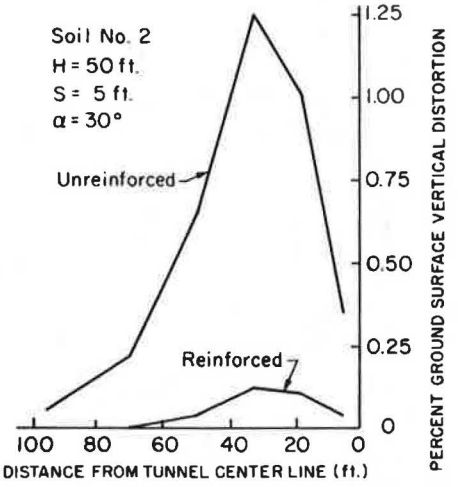

stance a reduction of 34 percent in surface settlement above the tunnel center can be achieved by reducing spile spacing from 4 ft to 2 ft, whereas approximately 29 percent and 6 percent reduction in crown and bottom movements are expected. Generally, the effect of spile spacing on the performance of the system, including tunnel deformations and ground surface movements, is much greater in weaker soils. Even though the effect of spile spacing is smaller in stronger soils, the reinforcing effect is still remarkable when the behavior of the reinforced system is compared with that of the unreinforced system.

The location of the potential failure surface was estimated by observing the variation of the maximum shear strains obtained from three-dimensional strains. A typical maximum shear strain distribution is depicted by the contours in Figure 10. The potential failure surface was approximated by connecting the highest maximum shear strain points. This indicates that the potential failure surface passes more or less through the side of the tunnel and propagates upward forming a circlelike curved surface as shown in Figure 10. The potential failure surface may be approximated in the design of the system by a series of straight lines or a continuous curve.

CONCLUSION

An investigation of a spiling reinforcement system used in soft-ground tunneling is described. A generalized plane strain finite-element analysis has been developed to calculate the three-dimensional stresses and displacements while the finite-element grid remains in two dimensions. From the information obtained from the analysis, effects of the reinforcement, the inclination, and the spacing of the spiles on the performance of the system have been discussed and quantified.

The developed method of analysis can be used for the calculation of tunnel and ground surface movements under various field conditions (e.g., soil type, tunnel depth, inclination and spacing of the spiles, and tunnel diameter). The results can then be used for the design of the spiling reinforcement system. An appropriate spile spacing can be chosen from the results to ensure that the deformation characteristics of the system can be kept within acceptable bounds. Because the method of analysis produces three-dimensional displacements, the out-of-plane direction displacement can be included in the calculation of the ground surface distortions. Figure 11 is an example that indicates the variation

Figure 9. Tunnel deformation for different spile inclinations.

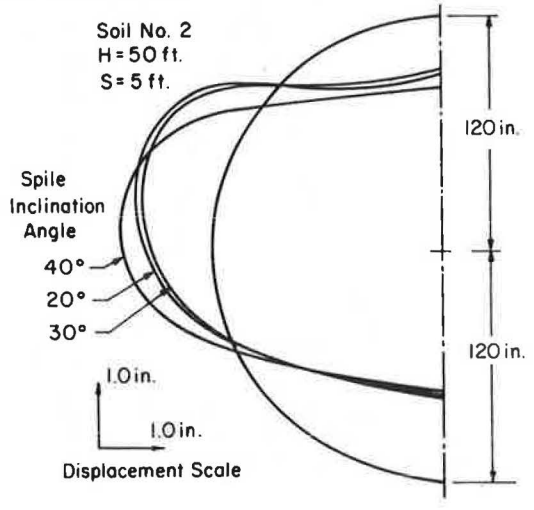

Figure 10. Contours of maximum shear strain.

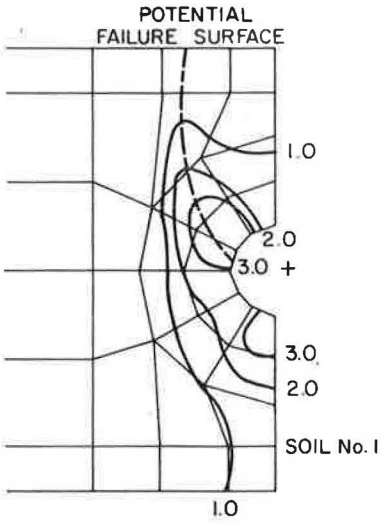

Figure 11. Variation of ground angular distortion.

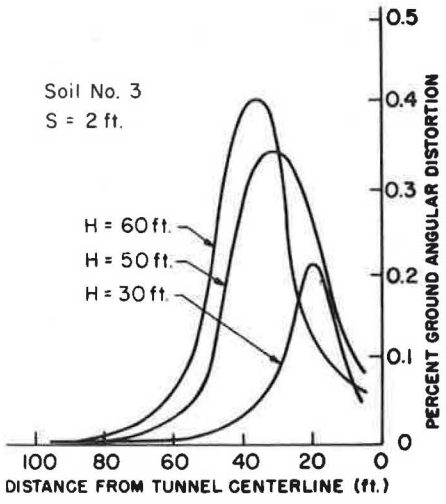

Table 3. Tunnel deformation with different spile spacings in soil No. 3 (H = 50 ft).

Spile Spacing (ft)	Crown (in.)	Bottom (in.)
5	-2.37	1.78
4	-2.29	1.76
3	-2.19	1.74
2	-1.65	1.65

of ground surface angular distortion, a measure of combined vertical distortion in three dimensions. Angular distortion can be obtained from

$$\text{Angular distortion} = (1/L)(\Delta\delta_y^2 + \Delta\delta_z^2)^{1/2} \quad (21)$$

where

L = distance between nodes,
$\Delta\delta_y$ = differential vertical displacement, and
$\Delta\delta_z$ = differential out-of-plane displacement.

The developed method of analysis was intended to capture the most essential characteristics involved in the spiling reinforcement system in soft-ground tunneling without resorting to three-dimensional grids. However, the validity of the developed method of analysis remains to be tested. Further research should be done in areas such as field instrumentation and monitoring of prototype systems or large-scale centrifuge model testing. In this way the validity and effectiveness of the developed analytic methods can be checked and extended.

ACKNOWLEDGMENTS

The work presented in this paper is based on research supported by the U.S. Department of Transportation under contract No. DTRS-5681-C-00024. The author is extremely grateful for this support.

REFERENCES

1. G.E. Korbin and T.L. Brekke. Field Study of Tunnel Prereinforcement. Journal of Geotechnical Engineering Division, ASCE, Vol. 104, No. GT8, 1978.
2. K.M. Romstad, L.R. Herrmann, and C.K. Shen. Integrated Study of Reinforced Earth-I: Theoretical Formulation. Journal of Geotechnical Engineering Division, ASCE, Vol. 102, No. GT5, 1976.
3. J.M. Duncan and K.S. Wong. Hyperbolic Stress-Strain Parameters for Non-Linear Finite Element Analysis of Stress and Movements in Soil Masses. University of California, Berkeley, Rept. TE-74-3, 1970.
4. E.J. Cording and W.H. Hansmire. Displacements Around Soft Ground Tunnels. 5th Panamerican Congress on SM & FE, Session IV, General Rept., Buenos Aires, Nov. 1975.
5. G.E. Korbin and T.L. Brekke. Model Study of Tunnel Prereinforcement. Journal of Geotechnical Engineering Division, ASCE, Vol. 102, No. GT9, 1976.
6. J.B. Burland and C.P. Wroth. Settlement of Buildings and Associated Damage. Proc., Conference on Settlement of Structures, 1975.
7. R. Grant, J.T. Christian, and E.H. Vanmarcke. Differential Settlement of Buildings. Journal of Geotechnical Engineering Division, ASCE, Vol. 100, No. GT9, 1974.
8. J. Kreisel. Fifteenth Ranken Lecture: Old Structure in Relation to Soil Conditions. Geotechnique, Vol. 25, No. 3, 1975.
9. D.E. Polshin and R.A. Tokar. Maximum Allowable Non-Uniform Settlement of Structures. Proc., 4th International Conference on SM & FE, Vol. 1, 1957.
10. A.W. Skempton and D.H. MacDonald. Allowable Settlement of Buildings. Proc., Institution of Civil Engineers, Part 3, Vol. 5, 1956.
11. L. Bjerrum. Discussion. Proc., European Conference on Soil Mechanics and Foundation Engineering, Vol. II, Wiesbaden, 1963.
12. T.D. O'Rourke, E.J. Cording, and M. Boscardin. The Ground Movements Related to Braced Excavation and Their Influence on Adjacent Buildings. U.S. Department of Transportation, Rept. DOT-TST-76T-23, Aug. 1976.

Publication of this paper sponsored by Committee Subsurface Soil-Structure Interaction.

Compactive Prestress Effects in Clays

ALBERT DiBERNARDO AND C.W. LOVELL

The load-deformation behavior of natural clays is strongly influenced by the geologic maximum past pressure. If such clays are excavated and manipulated before compaction, the geologic effect is largely lost. However, the compaction process establishes a new prestress value, and the ratio of this prestress to the effective normal stress in a compacted fill forms a new overconsolidation ratio (OCR). If the material and compactive prestress values are held constant in a moderately high embankment, the OCR values range from quite high at lesser depths to unity in lower embankment locations. Consequently, the nature of the shearing and compressibility responses varies considerably with position in the embankment. Laboratory studies have been conducted on both compacted shales and clays to demonstrate the empirical prediction of the prestress value and its relative effect on saturated compressibility and undrained shear behavior. The prestress varies with the nominal compaction pressure and its rate of application, as well as with the material and its water content. This value is predicted from the conventional oedometer test on the as-compacted material. When the compacted materials are soaked at a variety of confining pressures, which simulate differing embankment positions, the volume changes are highly dependent on the major compaction variables and the prestress. To achieve a homogeneous and predictable load-deformation response in major embankments, it is necessary to better understand and control the prestress effected by compaction. The research discussed here was conducted to examine the compressibility behavior of a laboratory-compacted soil in the as-compacted and soaked condition. A highly plastic residual clay and a kneading type of compaction were used. To determine the as-compacted compressibility characteristics, the compacted samples were trimmed to appropriate size and incrementally loaded in the oedometer. Of particular interest was the value of compactive prestress.

Early hypotheses concerning compaction of fine-grained soils explained the compaction process in terms of a predominant influence of individual clay particles (or clusters). More recently, the role of agglomerations or peds of clay particles has been emphasized.

BACKGROUND

Compaction Hypotheses

Barden and Sides (1) attempted to relate the engineering behavior of compacted clay to its fabric. Photomicrographs of the fabric of two clays revealed that the main difference between samples compacted